ЛЁД И СНЕГ, 2025, том 65, № 2, с. 357–372

ПРИКЛАДНЫЕ ИССЛЕДОВАНИЯ

УДК 551.321.1

ANALYSIS OF ICE CUTTINGS COLLECTED DURING DRILLING OF THE SNOW-FIRN LAYER AT VOSTOK STATION

© 2025 D. A. Vasilev*, I. V. Rakitin, S. A. Ignatev, A. V. Bolshunov, A. Yu. Ozhigin

Saint Petersburg Mining University, Saint Petersburg, Russia
**e-mail: Vasilev_da@pers.spmi.ru*

Received December 4, 2024; Revised December 24, 2024; Accepted April 18, 2025

The size and shape of the ice cuttings influence the choice of drilling regimes, as well as the design of drilling heads, augers, chip chambers, and internal drilling channels. To collect ice chips, two boreholes, VK-22 (30 m) and VK-23 (40 m), were drilled at Vostok station. Sieving was used to analyze the particle size distribution of the ice cuttings at full depth in both boreholes. The shape of the ice particles was examined microscopically at drilling depths of 5, 10, 15, 20, 25, 30, and 35 m of VK-23. The density of the snow-firn layer and the bulk density of ice cuttings were measured. The ice cuttings became finer-grained as the borehole depth increased. The prevailing fraction changes from 1.6–3 mm to 0.4–0.63 mm, the average particle diameter reduces from 1.55 mm to 0.06 mm, and the $D10$, $D50$, and $D90$ values decrease more than twice. The shape analysis revealed that the ice chips are dominated by equant and elongated particles, with medium shape projections described by parameters $FF = 0.74$ and $ER = 0.67$. A visual comparison of microscopic images shows that the thickness of the ice cuttings decreases as the depth of the well increases.

Keywords: Antarctic, ice drilling, snow-firn layer, ice cuttings, size distribution, shape characteristics

DOI: 10.31857/S2076673425020124, **EDN**: FOALPV

INTRODUCTION

A comprehensive study of the Antarctic ice sheet, subglacial lakes and bedrock is impossible without drilling, which is carried out as part of geological (Goodge at al., 2021), paleoclimatic (Veres et al., 2023), glaciological (Mikhalenko et al., 2024), microbiological (Ren et al., 2022), and other types of research. Ice drilling for scientific reasons has been going on for more than 150 years (Clarke, 1987), during which time tens of thousands of meters of boreholes have been bored all over the world, and the advancement of glacier drilling equipment and methods continues today. One of the many urgent problems in the field of ice drilling is increasing the efficiency of snow-firn layer (*SFL*) drilling, which is the most frequently drilled horizon of glaciers, as ice drilling begins at the surface, regardless of the final depth. The two most common methods of *SFL* core drilling are auger drilling and thermal drilling. The negative aspects of thermal drilling involve low energy efficiency, low rate of penetration (ROP), and heat impact on the ice core (Serbin, Dmitriev, 2022). These drawbacks led to the gradual decline in popularity of this drilling method. At the same time auger drilling has proven to be the most reliable method for drilling *SFL*. However, there is an unresolved problem with optimizing drill design parameters, which results in a significant decrease in length of drilling run as borehole depth increases (Talalay, 2016). The prospective direction in the field of high efficiency *SFL* drilling is mechanical air drilling. While air ice core drilling is still in its early stages (Hu et al., 2019; Ignatiev et al., 2023), noncoring drilling technologies (Gibson et al., 2020) are successfully used today.

One of the keys to increasing the efficiency of *SFL* drilling is a thorough understanding of the byproducts of the mechanical drilling (ice cuttings). By its nature, ice cuttings are a granular material, with the bulk density, size, and shape of the particles determining the majority of their physical and mechanical properties. Studies on the shape and size of drilled cuttings have been widely presented in the fields of exploration and oil drilling (Kyzym,

2015; Kern et al., 2022). At the same time, ice chips analysis was carried out only in two studies. Talalay (2006) provides data on how the ice particle size distribution (PSD) varies with depth of cut. Hong et al. (2015) investigate the effect of ROP and rotation frequency on the size and shape parameters of ice cuttings. Both papers focused on ice chips from drilling an artificial frozen ice block, which have a significantly different petrographic structure and thermobaric properties than the snow, firn or ancient atmospheric ice of Central Antarctica and Greenland.

The density, strength, porosity and petrostructural properties of the *SFL*, which have varied with depth over thousands of years under dry metamorphism, are extremely difficult to reproduce in laboratory conditions. Therefore, ice cuttings collected during drilling of the upper 40 m of *SFL*, the characteristics of which were previously unknown, were selected for the study. The article presents the results of experimental work carried out at Vostok station during seasons 67th, 68th, and 69th of the Russian Antarctic expeditions, in which the dependencies of the PSD, form parameters, and bulk density of ice chips on the ROP and density of the *SFL* at the constant rotation frequency of the drill were investigated. Based on the research results, the authors propose a vision for how the obtained data could be applied in the field of glacier drilling.

STUDY AREA

Vostok station is located in the central part of East Antarctica (78°28 S, 106°48 E) at an altitude of 3488 m and 1260 km from the coast (Litvinenko, 2020). The average temperature in the summer months, December and January, is −35.1 °C and −35.5 °C, and the coldest month, August, is 75.3 °C. Furthermore, the Vostok station area receives almost no precipitation, the average annual snow accumulation rate since 1970 has been 22.5 kg/m^2 (Ekaykin et al., 2023). Average annual atmospheric pressure: 624.2 gPa, relative humidity: 71% (Kapustin, 2018).

Since its foundation on December 16, 1957, a wide range of research has been carried out at the station. The most significant scientific achievement might be considered the drilling of the deepest borehole in ice and the unsealing of the subglacial Lake Vostok on February 5, 2012 (Litvinenko at al., 2020). The more than 440.000-year-old ice cores have allowed us to receive a continuous paleoclimate signal, significantly expanding our understanding of past climate. Since 1970, the Vostok station has been carrying out the most extensive instrumental snow accumulation observations for Central Antarctica (Ekaykin et al., 2023). Because of its proximity to the geomagnetic pole, Vostok station is ideal for conducting geophysical studies of the Earth's magnetic field. There was conducted vertical ionosphere sensing, regular meteorological observations and ozonometry.

MATERIALS AND METHODS

Sampling of cores and ice cuttings. The material for the experimental studies was samples of ice cuttings and cores obtained as a result of drilling the *SFL* in the area of Vostok station. Sampling was conducted from boreholes VK-22 (78°28′1″ S, 106°51′30″ E) (Ignatiev et al., 2023) and VK-23 (78°28′18″ S, 106°50′48″ E) (Bolshunov et al., 2023) which were drilled during the seasonal operations of the 67th, 68th, and 69th Russian Antarctic expeditions. The placement of the boreholes in relation to the Vostok station and the building site of the new wintering complex was chosen in such a way as to exclude the influence of artificial snow accumulation on the interpretation of the drilling results.

Drilling was carried out using an LGGE (Laboratorie de Glaciologie et Géophysique de l'Environnement) (Veres et al., 2020) drilling rig.

After each drilling run (the run was set to 0.5 m), samples of cuttings and cores were extracted and then packed into separate bags that were tagged in accordance with the run number and drilling interval. The cuttings and cores were delivered to the glaciological laboratory of the 5G borehole drilling complex, where they were stored at a temperature of −53 °C.

The drill head is equipped with two rounded cutters, one for each auger flight. The drill's penetration rate was manually controlled and measured every 5 meters of drilling. The drilling head rotation frequency was constant at 105 rpm.

The density of SFL. Despite the fact that the *SFL* density in the Vostok station area has been well studied (Ekaykin et al., 2022), in order to increase the reliability of the experimental studies, we decided to construct our own density profile for two boreholes, VK-22 and VK-23, to improve the reliability of the experimental studies.

The density profile of the *SFL* was performed using cores. Measurements were taken at 0.5 m intervals, starting at a depth of 5.5 m. The upper section of the *SFL* (0–5.5 m) had severely fractured and irregularly shaped cores, making density measurements impossible. Density calculations were performed using the equation:

$$\rho = \frac{m_c}{\pi \frac{D_c^2}{4} l_c},$$

where: m_c – core mass, kg; D_c – core diameter, m; l_c – core length, m.

The core diameter was calculated as the arithmetic mean of three measurements along the core length. The diameter and length of the core were measured using a caliper.

The confidence interval was calculated as ±2 *SEM* (standard error of mean):

$$SEM = \frac{STD}{\sqrt{n}},$$

where: *STD* – standard deviation of density values in the interval of 0.5 m according to data from two boreholes; n – number of values that fall into the interval (Ekaykin et al., 2022).

PSD analysis by sieving. Sample analysis of cuttings and cores was performed at the glaciological laboratory of the drilling complex of 5G borehole (average temperature −20 °C), equipped with a dedicated workspace (Ignatiev et al., 2023).

To determine the distribution of ice cuttings by size a sieve analysis method was used. The sieve analysis was carried out in a dry manner using a set of manual laboratory sieves with cell sizes of: 1.6, 1.25, 1, 0.8, 0.63, 0.4, 0.25 mm. The sieves were arranged in a column from the largest cell to the smallest from top to bottom. Thus, 8 fractions were determined: 1.6–3, 1.25–1.6, 1–1.25, 0.8–1, 0.63–0.8, 0.63–0.4, 0.25–0.4, 0–0.25 (the upper size limit of 3 mm was found experimentally; no cuttings larger than 3 mm were found at any drilling depth).

Sample mass measurements (as well as subsequent core mass measurements) were carried out using electronic scales with an error of ±0.1 g. The ice cuttings samples were prepared using the quartering method. The mass of one cuttings sample was 0.2 kg and sieving time – 1 min. A sieve analysis of the cuttings from VK-22 borehole was conducted at 0.5 m intervals in depth, for VK-23 borehole the interval was 2 m. The weight percentages of different fractions were calculated using the equation:

$$Q_i = \frac{m_i \cdot 100}{\sum m_i},$$

where: m_i – fraction mass.

The fractional composition was determined from three independent samples, which were sequentially sieved on sieves. The weight percentages of the fractions for each drilling interval were deduced from the sieving results.

For analyzing data on PSD, differential curves were used, constructed according to the values of fractional density (ISO 9276–1:1998), determined from the following equation:

$$q_m = \frac{Q_i}{d_1 - d_2},$$

where d_1 and d_2 – maximum and minimum sieve mesh sizes of the i^{th} fraction, mm

Using fractional density allows comparing the obtained results with the data presented in other studies. In the practice of describing differential curves, Gaussian (1) and lognormal (2) distribution laws are most commonly used (Dengaev et al., 2023):

$$F_G(d) = \frac{100}{\sigma\sqrt{2\pi}} \exp\left\{-\frac{1}{2}\left(\frac{d-\bar{d}}{\sigma}\right)^2\right\}, \quad (1)$$

where $\bar{d}$ – mean diameter of particle, mm; σ – standard deviation.

$$F_L(\ln d) = \frac{100}{d \ln\sigma_g \sqrt{2\pi}} \exp\left\{-\frac{1}{2}\left(\frac{\ln d - \ln\overline{d_g}}{\ln\sigma_g}\right)^2\right\}, \quad (2)$$

where $\overline{d_g}$ – geometric mean; σ_g – geometric standard deviation.

A parameter of the weighted average particle diameter of a bulk mass was used to calculate sieve analysis indicators. This parameter takes into account the influence of each fraction content on the final diameter value, which allows for the most accurate description of the particle sample. This parameter is determined by the following equation:

$$D_w = \frac{\sum_{i=1}^{n}(Q_i \cdot d_i)}{\sum_{i=1}^{n} Q_i},$$

where d_i – arithmetic mean diameter, mm.

The arithmetic mean diameter of the class is determined from the equation:

$$d_i = \frac{d_1 + d_2}{2}.$$

The applicability of a particular mathematical distribution to describe the composition of a specific dispersed system is mainly determined by the way this system is obtained. For example, the distribution of particles by sizes obtained during comminution (grinding, crushing, and milling) is very close to logarithmically normal. However, scattered systems (such as grains, cereals, and sand) that have not been forced by comminution are more likely to be distributed in accordance with a Gaussian law (Merkus, 2009).

For statistical analysis of PSD, parameters such as mass percentiles $D10$, $D50$, and $D90$ were used. These parameters are commonly used to describe bulk materials, including drill cuttings (Kern et al., 2022, Zhang et al., 2021). The values of percentiles are derived from a cumulative graph of PSD, which is constructed by sequentially summing the weight percentages of fractions and plotting a cumulative curve (Merkus, 2009).

Shape parameters. Particle shape parameter determination was carried out using the static image analysis method (ISO 13322-1:2014). Images of ice chips from borehole VK-23 were taken from depths of 5, 10, 15, 20, 25, 30 and 35 meters. For this purpose, cuttings from each depth were pre-sieved through sieves of sizes 1.6, 1.25, 1, 0.8, 0.63 and 0.4 mm. This process was followed by photography. Samples of coarse particles (fractions 1.6–3, 1.25–1.6, 1–1.25 mm) were placed between two polarized filters and photographed using a digital camera without magnification devices. Samples of fine particles (fractions 0.8–1, 0.63–0.8, 0.4–0.63 mm) were placed on glass slides and photographed under 40x magnification using a Levenhuk MED D10T LCD microscope. The study of particle shape parameters for fractions 0.25–0.4 mm and 0–0.25 mm, which represent a fine-dispersed material subjected to agglomeration, was not carried out due to methodological difficulties in analyzing particle conglomerations under a microscope. For the analysis of microphotographs, the open-source software ImageJ was used. The main geometric parameters of particles were determined as follows: the projected area of the particle (S_p, mm^2); the perimeter of the particle projection (P_p, mm); the major axis (l_max, mm) and the minor axis (l_min, mm) of the particle.

For the analysis of particle shape parameters of form factor (also known as "circularity" in the literature) and roundness (ellipse ratio) were utilized. The form factor parameter (*FF*) takes into account the ratio of the particle's projected area to its perimeter:

$$FF = \frac{4\pi \cdot S_\text{p}}{P_\text{p}^2}.$$

The roundness (*ER*) can be determined by the ratio of the area to the major axis or by the ratio of the minor axis to the major axis:

$$ER = \frac{4S_p}{\pi \cdot {l_\text{max}}^2} \approx \frac{l_\text{min}}{l_\text{max}}.$$

At a high value of the *FF* parameter, the particle shape is round and does not have sharp angles. Conversely, a low value of the parameter results in the opposite effect. The *ER* parameter is responsible for the compactness of the particle. A value of *ER* close to one indicates that the particle's elongation in two mutually perpendicular directions is almost equal, and vice versa.

To establish the relationship between changes in the shape of ice particles with increasing borehole depth, average weighted values of *FF* and *ER* were determined, taking into account the size distribution at each drilling interval:

$$FF_l = \frac{\sum_{n=1}^{i}(FF_i \cdot Q_{m_i}/100)}{\sum_{n=1}^{i} Q_{m_i}/100},$$

where: FF_i – arithmetic mean form factor of different particles fractions;

$$ER_l = \frac{\sum_{n=1}^{i}(ER_i \cdot Q_{m_i}/100)}{\sum_{n=1}^{i} Q_{m_i}/100},$$

where: ER_i – arithmetic mean ellipse ratio of different particles fractions.

Bulk density of ice cuttings. The methodology for analyzing the bulk density of ice cuttings involved using a technique for determining the density of bulk materials, utilizing a stand consisting of a Bunsen stand with a laboratory funnel attached to it. A laboratory beaker was placed under the funnel, with its volume chosen based on the volume of the ice cuttings sample being studied. When the ice cuttings sample was poured into the funnel, it would flow into the beaker under its own weight. The ice cuttings were poured into the funnel until the beaker was filled, excess volume (mound) was then removed, and the mass of the beaker was measured. The bulk density was determined using the equation:

$$\rho_b = \frac{m_f - m_e}{V},$$

where: m_f – mass of a full glass, kg; m_e – empty glass mass, kg; V – glass volume, m^3.

Measurements of bulk density for the ice cuttings from borehole VK-22 were carried out at intervals of 0.5 m depth, while for borehole VK-23, the interval was 2 m. The bulk density was determined based on three independent samples from each interval, and the average value was calculated. Additionally, the bulk density of separate fractions from borehole VK-22 was measured, and the obtained data were used in the study of the process of transporting ice cuttings by air (Ignatiev et al., 2023).

RESULTS

Sampling of cores and ice cuttings. Two boreholes, VK-22 (30 m) and VK-23 (40 m), were drilled, with a core recovery rate of 100% starting from a depth of 5.5 m. Samples of ice cuttings were collected from each run, with a cuttings output of approximately 1 kg per 0.5 m of drilling.

The results of SFL density measuring. The data on the dynamics of the growth of *SFL* density obtained from cores from VK-22 and VK-23 boreholes have a high degree of correlation and correspond to the data obtained during drilling of VK-16 (70.20 m), VK-18 (55.14 m) and VK-19 (65.37 m) boreholes (Veres et al., 2020).

As can be seen from the Fig. 1, *a*, up to a depth of 22 m, the spread of density values is quite high. The maximum value of the standard deviation was 41.5 kg/m^3. This is explained by the natural spatial variability of *SFL* density, which is formed in the process of the deposition of freshly fallen snow on the surface of the snow cover. With an increase in the depth of the firn and the achievement of a density of 450–500 kg/m^3, the spread of the density values decreases significantly, and the values of the standard deviation of measurements do not exceed the instrumental error.

The *SFL* density according to data from two boreholes is described by a cubic polynomial:

$$\rho_{SFL} = 0.0048x^3 - 0.435x^2 + 18.52x + 275.04,$$

where: x – borehole depth.

The obtained equation describing the change in *SFL* density, combined with ROP measurements during drilling, allows us to construct a graph describing a decrease in ROP as the density of the drilled *SFL* increases (see Fig. 1, *c*).

PSD analysis by sieving. Sieve analysis of the ice cuttings for VK-22 and VK-23 boreholes was carried out at 59 and 20 drilling intervals, respectively, the total number of measurements was 237.

Fig. 2, *a* presents the result of the mathematical analysis of the obtained data. It has been found that

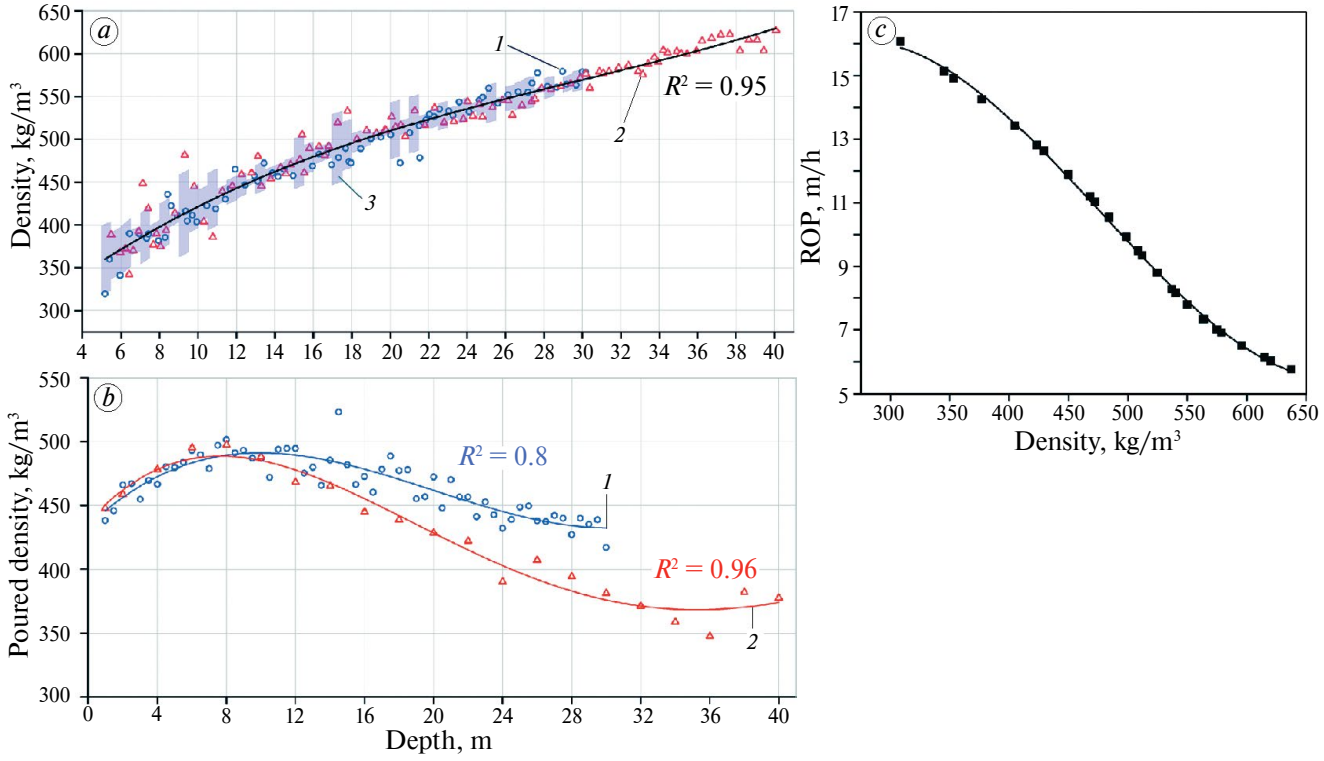

Fig. 1. Snow-firn layer density profile in Vostok station area (*a*); dependence of bulk density of ice cuttings on borehole depth (*b*); *1* – data obtained from VK-22 borehole (blue circles); *2* – data obtained from VK-23 borehole (red triangles); *3* – confidence interval ±2 *SEM* (blue shading); dependence of the rate of penetration on the density of the snow-firn layer (*c*)

Рис. 1. Профиль плотности снежно-фирновой толщи в районе станции Восток (*a*); зависимость насыпной плотности ледяного шлама от глубины скважины (*b*); *1* – данные, полученные из скважины VK-22 (синие круги); *2* – данные, полученные из скважины VK-23 (красные треугольники); *3* – доверительный интервал ±2 *SEM* (голубая заливка); зависимость механической скорости бурения от плотности снежно-фирновой толщи (*c*)

the PSD up to a depth of 15 m obeys the Gaussian distribution law, while at deeper depths it obeys a log-normal distribution, which is true for both boreholes. Fig. 2, *b* presents the cumulative curves of PSD. With increasing borehole depth, the shape of the distribution curves changes from concave to convex, indicating an increase in the proportion of particles of small size fractions. According to these curves, the values of *D*10, *D*50, and *D*90 parameters were determined (indicated in red on the abscissa axis).

As can be seen from Fig. 2, *c*, the percentile values decrease with increasing borehole depth. For VK-22, the percentile values of *D*10, *D*50 and *D*90 decreased by 52, 53 and 56%, respectively, with an increase in borehole depth from 5 to 30 m. Similar values for the same drilling interval for the VK-23 borehole are 54, 52 and 56%, which demonstrates a high correlational dependence of changes in the granulometric composition of the ice chips in the two boreholes. The average diameter of particles also decreases by half with increasing depth.

Based on the *D*90 percentile values (from 1.18 to 2.59), samples of ice cuttings can be classified as a coarse-grained (from 1 to 10 mm) polydisperse system (see Fig. 2, *c*). The width of the PSD function, determined by the ratio of the *D*90 and *D*10 parameters, increases with depth from "medium" (from 1.5 to 4) to "wide" (from 4 to 10) (Merkus, 2009).

Fig. 3, *a* and Fig. 3, *b* present the dependences of the main parameters of the ice cuttings particle size (weighted average diameter, *D*50) on the ROP and *SFL* density.

Shape parameters. Based on the results of determining the shape parameters, the number of studied particles reached 5315 pieces. Analysis of all the studied particles, regardless of the drilling interval, shows that the patterns of distribution of *FF* and *ER* (Fig. 4) can be described by the law of normal distribution. Thus, for *FF*, the mathematical expectation (μ) and standard deviation (σ) equal 0.74 and 0.11, respectively. For *ER*, $\mu = 0.67$, $\sigma = 0.17$.

Based on the established patterns of shape parameters distribution, it is possible to conditionally distinguish four types of shapes. Particles for which the values of the shape parameters are close to unity should be considered as equant (Fig. 5, *a*). Particles slightly elongated in one direction are usually called rounded or rolled (see Fig. 5, *b*). Particles whose longest axis is 2–2.5 times the shortest are called elongated or oblong (see Fig. 5, *c*). The shape of particles in which one of the mutually perpendicular directions is much larger than the other is called rod-like (see Fig. 5, *d*) (Blott, Pye, 2007; Rodriguez et al., 2013). As can be seen from the graphs (see Fig. 4), rounded and elongated particles predominate in samples of ice cuttings from the VK-23 borehole.

Bulk density of ice cuttings. The bulk density of ice cuttings according to data from borehole VK-22, is described by a cubic polynomial:

$$\rho_b = 0.014x^3 - 0.87x^2 + 12.95x + 433.75,$$

where: x – borehole depth, m.

The bulk density of ice cuttings according to data from borehole VK-23, is described by a 4th degree polynomial:

$$\rho_b = -2.65 \cdot 10^{-4} x^4 + 0.034x^3 - 1.37x^2 + 15.40x + 436.47.$$

At a depth of 8 meters, the bulk density of ice chips from both boreholes increases with a high correlation of values, reaching 497–502 kg/m^3 (see Fig. 1, *b*). Following that, the bulk density decreased to the lowest values of 417.2 kg/m^3 and 347.6 kg/m^3 for VK-22 and VK-23, respectively.

DISCUSSION

Results. The geometric parameters of the drilling head and its rotation frequency speed remained constant during the drilling, implying that the petrostructural properties of the *SFL* and ROP are the primary factors affecting the size and shape of the ice cuttings.

Studies on the core from borehole VK-23 showed that the growth of the firn's ice grains is caused by recrystallization processes under directed stress and over time (Bolshunov et al., 2023). Lipenkov et al. (2007), based on the analysis of ice cores from deep boreholes, describe in detail the mechanism of firn grain growth in Vostok station area with increasing depth. According to their data, at a depth range of 10–40 m, the average size of firn grains increases from 1.15 to 1.25 mm. The rising ratio of the upper layers with depth increases the *SFL*'s strength and density. It was also found that as the depth of the borehole increases, the ROP decreases and is inversely related to the increasing density of the *SFL*. With the reduction of the penetration rate, the depth of cut decreases, which leads to a reduction in the size of ice particles, as demonstrated experimentally (Talalay, 2006; Hong et al., 2015). The medium diameter and *D*50 values decrease with depth, which is directly proportional to the ROP and inversely proportional to the density of the snow layer (see Fig. 3).

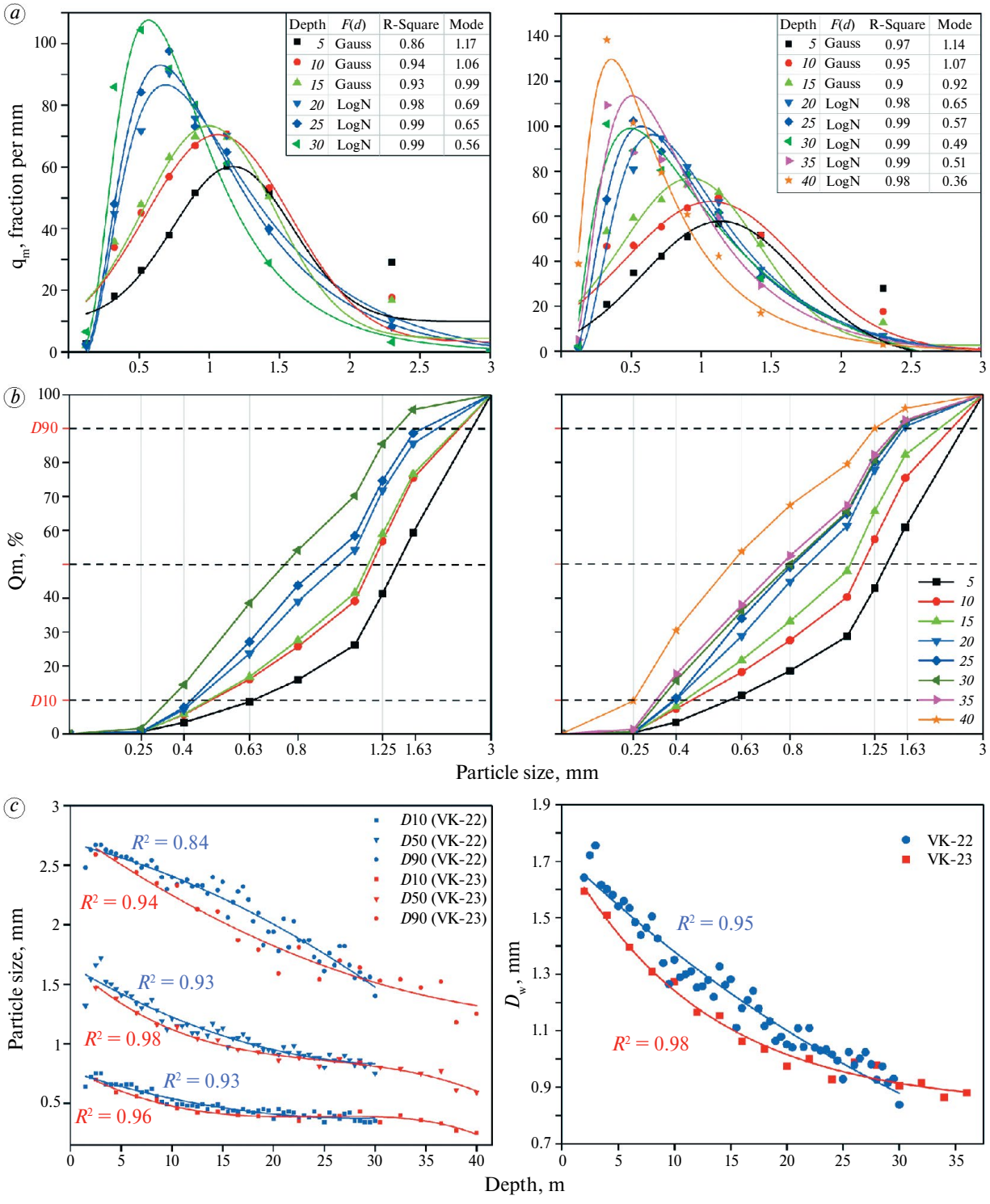

Fig. 2. Size parameters of ice particles, obtained from VK-22 and VK-23 boreholes. Data, obtained from different depths are indicated by colors and symbols in accordance with the legend on the charts: smoothed differential curves of particle size distribution (*a*); cumulative curves of particle size distribution (*b*); dependence of the values of percentiles *D*10, *D*50, *D*90 and weighted average particle diameter D_w on the borehole depth (*c*)

Рис. 2. Параметры размеров частиц, полученных из скважин VK-22 и VK-23. Данные, полученные с разных глубин, обозначены цветами и маркерами в соответствии с легендой на графиках. Цифровые обозначения в легенде означают исследуемую глубину бурения в метрах: дифференциальные кривые распределения частиц по размерам (*a*); кумулятивные кривые распределения частиц по размерам (*b*); зависимость значений процентилей *D*10, *D*50, *D*90 и средневзвешенного диаметра D_w от глубины скважин (*c*)

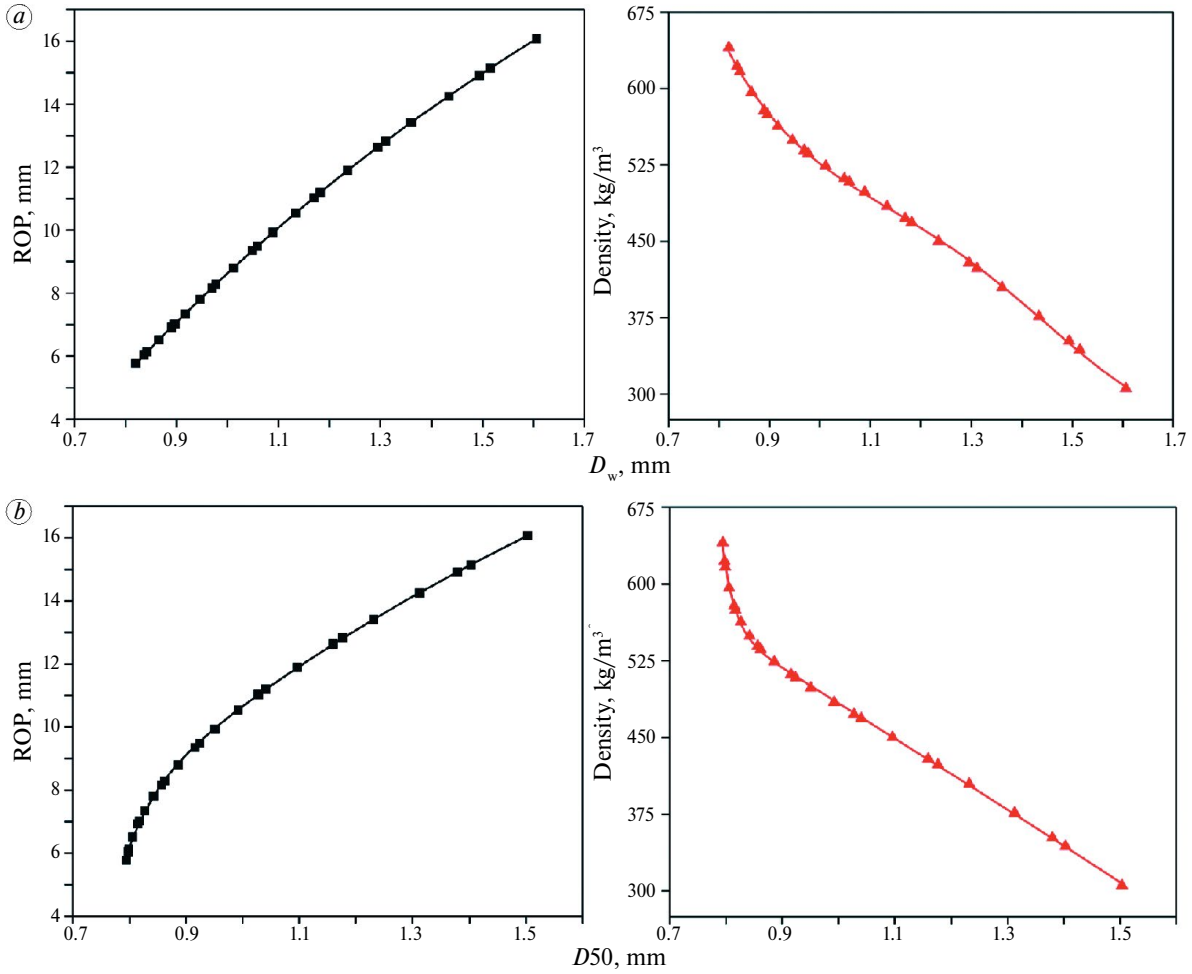

Fig. 3. Dependence of the weighted average diameter D_w on the rate of penetration and the density of the snow-firn layer (*a*); dependence of the percentile *D*50 on the rate of penetration and the density of the snow-firn layer (*b*)

Рис. 3. Зависимость средневзвешенного диаметра D_w от механической скорости бурения и плотности снежно-фирновой толщи (*a*); зависимость процентиля *D*50 от механической скорости бурения и плотности снежно-фирновой толщи (*b*)

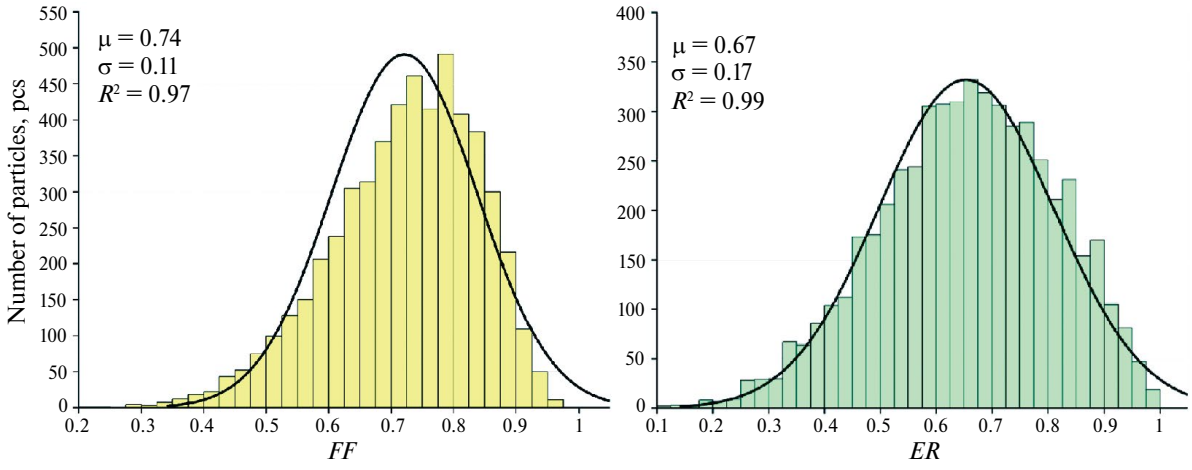

Fig. 4. Distribution of ice cuttings shape parameters values

Рис. 4. Распределение значений параметров формы частиц ледяного шлама

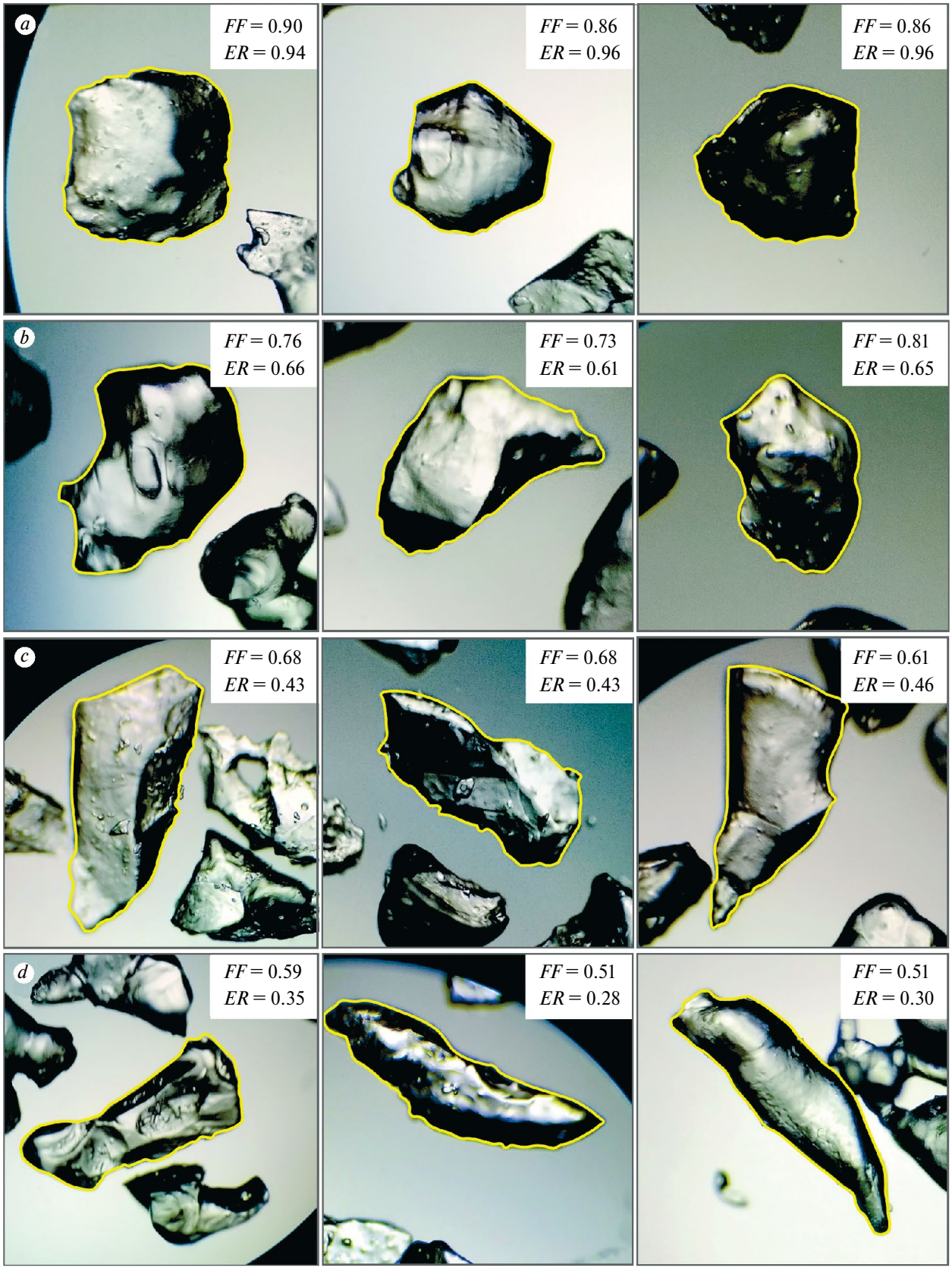

Fig. 5. Types of ice cuttings shapes: equant (*a*); rounded (*b*); elongated (*c*); rod (*d*)
Рис. 5. Типы форм частиц ледяного шлама: изометрическая (*a*); округлая (*b*); удлинённая (*c*); стержневая (*d*)

Thus, the change in size distribution as drilling depth increases can be explained by the fact that at shallow depths, ice grains have a greater degree of freedom and tend to separate from one another when a load is applied. As the drilling depth increases, the size of the firn's ice grains increases and the gaps between them decrease, the firn becomes denser and stronger. As a result, the effort required to separate one grain from the other is increased, which leads not only to the separation of grains along their borders, but also to their destruction by the drilling head's cutters, increasing the fineness of the chips. The fact that the law of size distribution changes as drilling depth increases lends support to this assertion (see Fig. 2, *a*). Up to a depth of 15 m, the normal law of distribution is observed, as is typical of particles that have not been crushed. At a drilling interval of 15–20 m, the distribution law shifts from normal to lognormal, this is typical for grinded particles, in this case by a drilling head. This claim is positively related to the fact that the predominant fraction varies with depth. At the start of drilling in both boreholes, the predominant fraction was 1.6–3 mm (up to 53.2% of the total sample mass), but as drilling depths increased (18 m for VK-22 and 16 m for VK-23) the dominant size became 1–1.25 mm. In the final stages of drilling (21.5 m for VK-22 and 20 m for VK-23) the highest mass percentage has particles with a size of 0.4 to 0.63 mm.

Despite the correlation of the values FF_l and ER_l, the analysis of the shape parameter measurement results revealed no clear pattern of change with increasing borehole depth. Therefore, the shape of the ice chips should be determined by analyzing all of the particles, regardless of the drilling depth. The parameters *FF* and *ER* vary in wide ranges ($FF = 0.22–0.97$; $ER = 0.1–0.99$), however, the mean values should be considered: $FF = 0.74$ and $ER = 0.67$ (see Fig. 4). If we give the mean *ER* value as the ratio of the major axis of the particle to the minor one, we get the number 1.49, which is similar to the value obtained by the Chinese colleagues (1.55) (Hong et al., 2015). The form parameters of ice particles are distributed according to the normal law, which is consistent with previous research on cuttings obtained from rock drilling (Zhang et al., 2021).

It should be noted that the optical microscopy method used in these studies does not allow for the measurement of particle thickness. However, micro-images of cuttings from the same fraction at different drilling depths can be compared (Fig. 6). As the borehole depth grows, the particles' transparency and light transmission increase, which means that the particles become more plate-shaped. This assertion is supported by a decrease in both the total bulk density (see Fig. 1, *b*), and the bulk density of individual fractions (Ignatiev and others, 2023). This is due to the fact that isometric particles at higher drilling depths occupy the same volume with fewer air gaps than plate-shaped particles at deeper depths.

An ellipsoid with axes $b > a > c$ can be used to approximate the shape of the ice particles to show this change in shape (Hong et al., 2015). According to the founded *ER*, the *a* axis has a 0.67 ratio to the *b* axis. The *c* axis is determined by the equation:

$$c = k \cdot b,$$

where k – thickness coefficient.

With increasing borehole depth, k varies from about 0.5–0.6 to 0.2–0.3 (see Fig. 6, *b*). This data can be applied in mathematical modeling of ice drilling processes. A 3D particle shape analysis is planned in the future to provide an accurate quantitative estimate of particle thinning (Rodriguez et al., 2013).

Practical importance. Analysis of ice cuttings collected during drilling of the *SFL* at Vostok station began as part of the work on developing drilling technology with air reverse circulation. Data on the shape and PSD of ice cuttings were used to investigate their suspension velocity (Ignatiev et al., 2023). Furthermore, the data obtained allowed us to calculate the geometric characteristics of the drill's internal channels, as well as the air flow and pressure required for effective bottomhole cleaning.

At the same time, the data collected may be useful in other projects aimed at developing ice drilling technologies. Thus, Hu et al. (2019) proposed using a filter screen with a mesh size of 0.2 mm when drilling the *SFL*. The theoretical efficiency of this filter can be easily calculated using the data obtained on the PSD of ice cuttings.

With the obtained data on the PSD of ice cuttings, it is easy to calculate the theoretical efficiency of this filter. Assuming that ice chips of the smallest fraction (0–0.25 mm) can pass through the mesh, the theoretical efficiency of the filter can be found by the formula:

$$\mu = 100 - Q_{0-0.25}.$$

Thus, the theoretical efficiency of the proposed screen filter will not fall below 98% up to a well depth of 36 m. However, further, the proportion of fine particles in the ice cuttings increases and at a depth

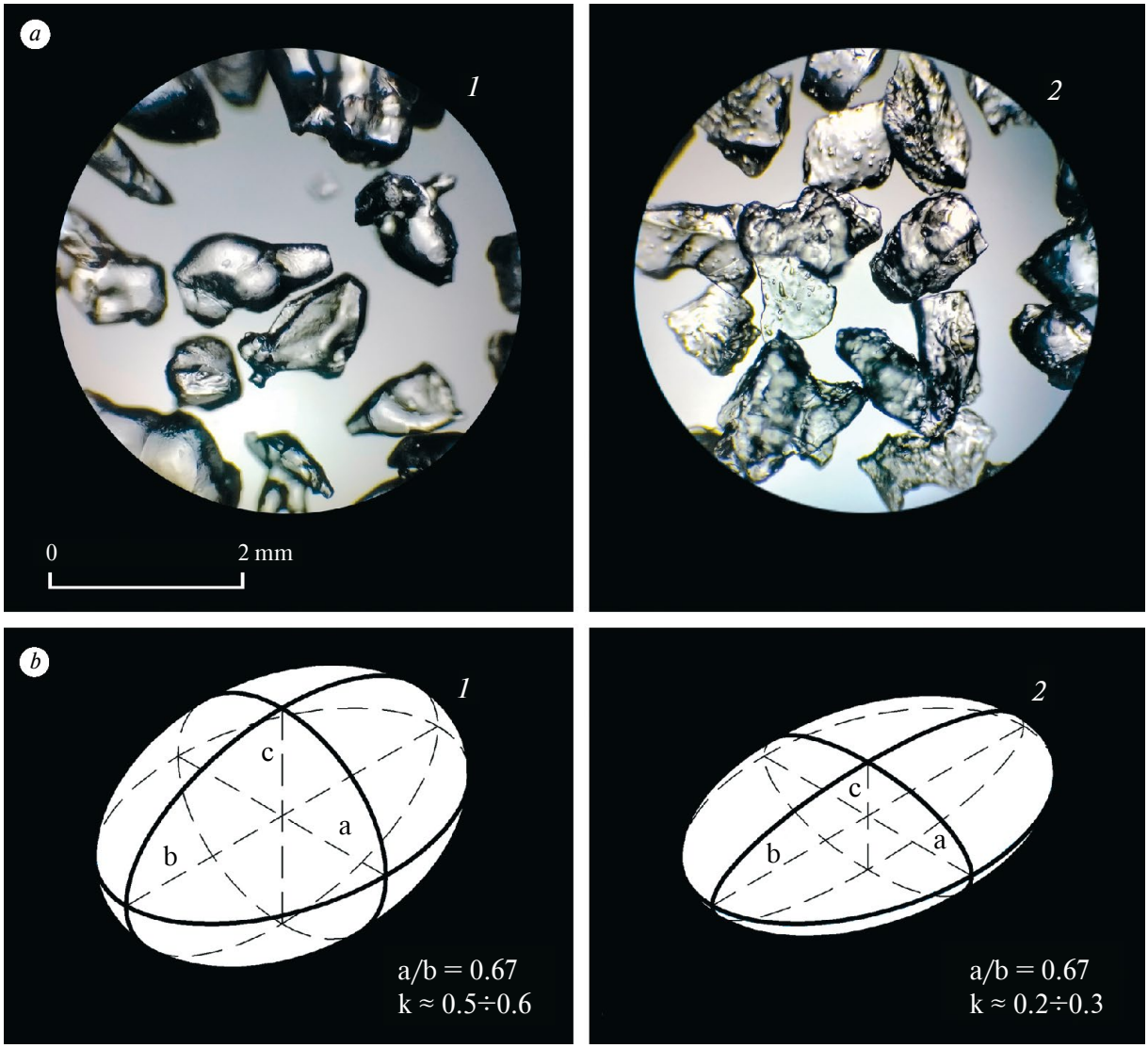

Fig. 6. 0.63–0.8 mm ice particles sampled at the different drilling depths (*a*); visual representation of ice cuttings dimensions approximation based on drilling depths; *1* – 5 m; *2* – 30 m (*b*)

Рис. 6. ледяной шлам крупностью 0.63–0.8 мм (*a*), отобранный на различных глубинах бурения; визуализация аппроксимированной геометрии частиц ледяного шлама с глубин; *1* – 5 м; *2* – 30 м (*b*)

of 40 m, the filter efficiency decreases to 90.3%. This means that almost ten percent of the mass of the ice chips formed at the bottomhole will pass freely through the filter, potentially causing ice seals to form in the drill's internal channels and ceasing air circulation. The authors recommend using cyclone filters for effective cuttings collection while air drilling, which have been experimentally proven to be more than 97% effective and do not depend on ice particle size (Bolshunov et al., 2023).

The obtained data on the density of *SFL* and the bulk density of ice cuttings allow us to calculate the fragmentation index:

$$n = \frac{\rho_{SFL}}{\rho_b}.$$

Up to a depth of 14 m n <1 (minimum value 0.74), this means that the ice chips occupy a smaller volume than the undisturbed snow-firn massif. As the depth of the borehole increases, *n* rises above zero, reaching a maximum of 1.72 at 36 m. Knowing how the fragmentation index changes with depth, it is possible to more accurately calculate the required volume of the chip chamber of the cable suspended drill or predict the volume of cuttings accumulating at the borehole top, as it happens when drilling with RAM and RAM-2 (Gibson et al., 2020).

The discrete element method (DEM) has recently been actively used in the development of ice drilling technologies. Hong and others (2014) studied the optimal rotation frequency of the drill and the auger flight angle of inclination using DEM modeling. The ROP was assumed to be constant (valid only for homogeneous ice), the size of the ice particles was determined by the cutting depth, and their shape was approximated to a sphere. The best results for ice cuttings transportation were found at 100 rpm and an angle of inclination of 35–40°. The data we obtained make it possible to further develop the model created by our Chinese colleagues, taking into account the discovered dependencies between ice cuttings size and ROP (see Fig. 3), as well as data on ice cuttings shape (see Fig. 4). For example, an ellipsoidal particle generates more friction, allowing it to be transported at a steeper angle of inclination of the auger flight. Similarly, the founded characteristics of ice cuttings may be used to improve the model made by Hou et al. (2024) that describes the interaction of ice core and chips in an ascending air flow.

CONCLUSIONS

The PSD of the ice cuttings changes with the increase in the depth of the borehole; the chips become more fine-grained, as evidenced by the results of sieve analysis. At the upper drilling interval (10–15 m), the predominant particle size is 1.6–3 mm, while at the depth of 20–22 m, the main fraction becomes 0.4–0.63 mm. The reduced particle size is also demonstrated by the $D10$, $D50$, and $D90$ dynamics, which have mean values that decrease more than twice as the depth of the borehole increases. The average particle diameter decreases by 44.5%, from 1.55 mm to 0.86 mm. At a depth of 20 m, the law of PSD shifts from normal to log normal, which could indicate an increase in the proportion of particles crushed during drilling. The average diameter of the ice particles and $D50$ were found to be directly proportional to the ROP and inversely proportional to the density of the *SFL*.

An analysis of the shape of ice particles showed that the cuttings are dominated by elongated and rounded particles, with the medium-shape projection described by the parameters $FF = 0.74$ and $ER = 0.67$. The *FF* values range from 0.22 to 0.97 and *ER* values from 0.1 to 0.99, and their distribution follows the normal law. Based on the microscope analysis and data on the bulk density of ice cuttings, it was discovered that particle thickness decreases with increasing drilling depth. A quantitative assessment of this fact is planned for the future, employing methods of 3D analysis.

The size and shape parameters of ice cuttings obtained from boreholes VK-22 and VK-23 show strong correlations. Furthermore, the results of prior research on ice chips are similar to the data collected, allowing us to assess the validity of the chosen method of study and the reliability of the results. The collected data can be used to improve existing and develop new ice drilling technologies. The authors have proposed several directions for the practical application of the research results.

Data availability. The information contained in the article is available on request at *Vasilev_DA@pers.spmi.ru*.

Acknowledgements. The authors thank the employees of the Climate and Environmental Research Laboratory, Arctic and Antarctic Research Institute, V.Ya. Lipenkov, A.V. Turkeev, A.A. Ekaykin, I.A. Alekhina, N.A. Tebenkova, and A.N. Veres, for their assistance in carrying out the present study. Separate thanks are extended to the Russian Antarctic expedition participants, V.N. Zarovchatsky, N.S. Krikun, A.V. Gajvaronsky and K.A. Ovchynnikov. We also thank the anonymous reviewers for helpful comments and advice.

The research was performed at the expense of the subsidy for the state assignment in the field of scientific activity for 2024 № FSRW-2024-0003.

Благодарности. Коллектив авторов выражает благодарность сотрудникам Лаборатории изменения климата окружающей среды В.Я. Липенкову, А.В. Туркееву, А.А. Екайкину, И.А. Алехиной, Н.А. Тебеньковой и А.Н. Верес за помощь в проведении представленного исследования. Отдельная благодарность выражается участникам Российской антарктической экспедиции В.Н. Заровчатскому, Н.С. Крикуну, А.В. Гайваронскому и К.А. Овчинникову. Мы также благодарим анонимных рецензентов за полезные комментарии и советы.

Исследование выполнено с помощью субсидии на выполнение государственного задания в сфере научной деятельности на 2024 г. № FSRW-2024-0003.

REFERENCES

Bolshunov A.V., Vasilev D.A., Dmitriev A.N., Ignatev S.A., Kadochnikov V.G., Krikun N.S., Serbin D.V., Shadrin V.S. Results of complex experimental studies at Vostok station in Antarctica. *Zapiski Gornogo instituta*. Journ. of Mining Institute. 2023, 263: 724–741. EDN: WQNJET [In Russian].

Ekaykin A.A., Tchikhatchev K.B., Veres A.N., Lipenkov V.Y., Tebenkova N.A., Turkeev A.V. Vertical profile of snow-firn density in the vicinity of Vostok station, Central Antarctica. *Led i Sneg.* Ice and Snow. 2022, 62 (4): 504–511. https://doi.org/10.31857/S2076673422040147 [In Russian].

Ignatiev S.A., Vasilev D.A., Bolshunov A.V., Vasileva M.A., Ozhigin A.Y. Experimental research of ice cuttings transport by air while drilling of the snow-firn layer. *Led i Sneg.* Ice and Snow. 2023, 63 (1): 141–152. https://doi.org/10.31857/S2076673423010076 [In Russian].

Kapustin A.V. Some peculiarities of production of meteorological measurements at antarctic station East. Colloquium-journal. 2019, 9 (33): 17–25. https://doi.org/10.24411/2520-6990-2019-10216 [In Russian].

Lipenkov V.Ya., Polyakova E.V., Duval P., Preobrazhenskaya A.V. Structural features of the Antarctic ice sheet in the area of Vostok station based on the results of petrostructural studies of the ice core. Arctic and Antarctic Research. 2007, 2 (76) 68–77 [In Russian].

Serbin D.V., Dmitriev A.N. Experimental research on the thermal method of drilling by melting the well in ice mass with simultaneous controlled expansion of its diameter. *Zapiski Gornogo instituta*. Journ. of Mining Institute. 2022, 257: 833–842. https://doi.org/10.31897/PMI.2022.82 [In Russian]

Veres A.N., Ekaykin A.A., Lipenkov V.Ya., Turkeev A.V., Khodzer T.V. First data on the climate variability in the vicinity of Vostok Station (central Antarctica) over the past 2000 years based on the study of a snow-firn core. *Problemy Arktiki i Antarktiki*. Arctic and Antarctic Research. 2020, 66 (4): 482–500. https://doi.org/10.30758/0555-2648-2020-66-4-482-500 [In Russian].

Blott S.J., Pye K. Particle shape: a review and new methods of characterization and classification. Sedimentology. 2007, 55 (1): 31–63. https://doi.org/10.1111/j.1365-3091.2007.00892.x

Clarke G.K.C. A short history of scientific investigations on glaciers. Journ. of Glaciology. 1987, (33) S1, 4–24. https://doi.org/10.3189/S0022143000215785

Dengaev A.V. Mechanical Impurities Carry-Over from Horizontal Heavy Oil Production Well. Processes. 2023, 11: 2932. https://doi.org/11.2932.10.3390/pr11102932

Ekaykin A.A., Lipenkov V.Ya., Tebenkova N. Fifty years of instrumental surface mass balance observations at Vostok Station, Central Antarctica. Journ. of Glaciology. 2023: 1–13. https://doi.org/10.1017/jog.2023.53

Gibson C. RAM-2 Drill system development: an upgrade of the Rapid Air Movement Drill. Annals of Glaciology. 2020, 62 (84): 1–10. https://doi.org/10.1017/aog.2020.72

Goodge J.W., Severinghaus J.P., Johnson J., Tosi D., Bay R. Deep ice drilling, bedrock coring and dust logging with the Rapid Access Ice Drill (RAID) at Minna Bluff, Antarctica. Annals of Glaciology. 2021, 62: 1–16. https://doi.org/10.1017/aog.2021.13

Hu Zh., Talalay P.G., Zheng Zh., Cao P., Shi G., Li Y., Fan X., Ma H. Air reverse circulation at the hole bottom in ice-core drilling. Journ. of Glaciology. 2019, 65: 149–156. https://doi.org/10.1017/jog.2018.95

Hong J., Fan X., Liu Y., Liu G., Liu B., Talalay P. Size distribution and shape characteristics of ice cuttings produced by an electromechanical auger drill. Cold Regions Science and Technology. 2015, 119: 204–210. https://doi.org/10.1016/j.coldregions.2015.08.012

Hong J., Talalay P., Sysoev M., Fan X. DEM modeling of ice cuttings transportation by electromechanical auger core drills. Annals of Glaciology. 2014, 55 (68): 65–71. https://doi.org/10.3189/2014AoG68A002

Hou Zh., Liu Y., Meng Q., Xu H., Liang N., Yang G. Investigation of the dynamic ascent characteristics of ice core during polar core drilling. Cold Regions Science and Technology. 2024, 222: 104184. https://doi.org/10.1016/j.coldregions.2024.104184

International Organization for Standardization. ISO 13322–1:2014 Particle size analysis – Image analysis methods – Part 1: Static image analysis methods, 2nd ed. Geneva: International Organization for Standardization, 2014.

International Organization for Standardization. ISO 9276–1:1998 Repre- sentation of results of particle size analysis – Part 1: Graphical representation, 2nd ed. Geneva: International Organization for Standardization, 1998.

Kern J., Montagna G., Borges M. Techniques for determining size and shape of drill cuttings. Brazilian Journal of Petroleum and Gas. 2022, 16 (2): 65–77. https://doi.org/10.5419/bjpg2022-0006

Kyzym I., Reyes R., Rana P., Molgaard J., Butt S. Cuttings Analysis for Rotary Drilling Penetration Mechanisms and Performance Evaluation. Conference: ARMA 2015. 49th US Rock Mechanics. 2015.

Litvinenko V.S. Foreword: Sixty-year Russian history of Antarctic sub-glacial lake exploration and Arctic natural resource development. Geochemistry. 2020, 80 (3). https://doi.org/10.1016/j.chemer.2020.125652

Litvinenko V.S., Leitchenkov G.L., Vasiliev N.I. Anticipated sub-bottom geology of Lake Vostok and technological approaches considered for sampling. Geochemistry. 2020: 80. https://doi.org/10.1016/j.chemer.2019.125556

Merkus H.G. Particle Size Measurements Fundamentals, Practice, Quality. Springer, 2009.

Mikhalenko V., Kutuzov S., Toropov P., Legrand M., Sokratov S., Chernyakov G., Lavrentiev I., Preunkert S, Kozachek A., Vorobiev M., Khairedinova A., Lipenkov V. Accumulation rates over the past 260 years archived in

Elbrus ice core, Caucasus. Climate of the Past. 2024, 20: 237–255. https://doi.org/10.5194/cp-20-237-2024

Ren Z., Gao H., Luo W., Elser J. Bacterial communities in surface and basal ice of a glacier terminus in the headwaters of Yangtze River on the Qinghai–Tibet Plateau. Environmental Microbiome. 2022, 17 (12): 1–14. https://doi.org/10.1186/s40793-022-00408-2

Rodriguez J., Edeskär T., Knutsson S. Particle shape quantities and measurement techniques: a review. The electronic journal of geotechnical engineering. 2013, 18: 169–198.

Talalay P.G. Removal of cuttings in deep ice electromechanical drills. Cold Regions Science and Technology. 2006, 44 (2): 87–98. https://doi.org/10.1016/j.coldregions.2004.08.005

Talalay P.G. Mechanical Ice Drilling Technology. Singapore: Springer, 2016

Veres A.N., Ekaykin A.A., Golobokova L.P., Khodzher T.V., Khuriganowa O.I., Turkeev A.V. A record of volcanic eruptions over the past 2,200 years from Vostok firn cores, Central East Antarctica. Front. Earth Sci. 2023, 11: 1075739. https://doi.org/10.3389/feart.2023.1075739

Zhang Z., Lan X., Wen G., Qingming L., Yang X. An Experimental Study on the Particle Size and Shape Distribution of Coal Drill Cuttings by Dynamic Image Analysis. Geofluids. 2021: 1–11. https://doi.org/10.1155/2021/5588248

Citation: *Vasilev D.A., Rakitin I.V., Ignatev S.A., Bolshunov A.V., Ozhigin A.Yu.* Analysis of ice cuttings collected during drilling of the snow-firn layer at Vostok station. *Led i Sneg.* Ice and Snow. 2025, 65 (2): 357–372. doi: 10.31857/S2076673425020124

АНАЛИЗ ЛЕДЯНОГО ШЛАМА, ПОЛУЧЕННОГО ПРИ БУРЕНИИ СНЕЖНО-ФИРНОВОЙ ТОЛЩИ НА СТАНЦИИ ВОСТОК

© 2025 г. Д. А. Васильев*, И. В. Ракитин, С. А. Игнатьев, А. В. Большунов, А. Ю. Ожигин

Санкт-Петербургский горный университет, Санкт-Петербург, Россия

**e-mail: Vasilev_da@pers.spmi.ru*

Поступила в редакцию 04.12.2024 г.
После доработки 24.12.2024 г.
Принята к публикации 18.04.2025 г.

Установлены и описаны зависимости изменения размера и формы ледяного шлама снежно-фирновой толщи района станции Восток с учётом плотности массива и механической скорости бурения. Предложена классификация формы частиц ледяного шлама и её аппроксимация к эллипсоиду. Рассмотрена практическая значимость полученных данных при разработке техники и технологий бурения верхних горизонтов ледников.

Ключевые слова: Антарктида, бурение во льду, снежно-фирновый слой, ледяной шлам, гранулометрический анализ, характеристики формы

СПИСОК ЛИТЕРАТУРЫ

Большунов А.В., Васильев Д.А., Дмитриев А.Н., Игнатьев С.А., Кадочников В.Г., Крикун Н.С., Сербин Д.В., Шадрин В.С. Результаты комплексных экспериментальных исследований на станции Восток в Антарктиде // Записки Горного института. 2023. Т. 263. С. 724–741. EDN WQNJET

Екайкин А.А., Чихачев К.Б., Верес А.Н., Липенков В.Я., Тебенькова Н.А., Туркеев А.В. Профиль плотности снежно-фирновой толщи в районе станции Восток, Центральная Антарктида // Лёд и Снег. 2022. Т. 62. № 4. С. 504–511. https://doi.org/10.31857/S2076673422040147

Игнатьев С.А., Васильев Д.А., Большунов А.В., Васильева М.А., Ожигин А.Ю. Экспериментальные исследования переноса ледяного шлама воздухом при бурении снежно-фирновой толщи // Лёд и Снег. 2023. Т. 63. № 1. С. 141–152. https://doi.org/10.31857/S2076673423010076

Капустин А.В. Некоторые особенности производства метеорологических измерений на

антарктической станции Восток // Colloquium-journal. 2019. № 9 (33). С. 17–25. https://doi.org/10.24411/2520-6990-2019-10216

Липенков В.Я., Полякова Е.В., Дюваль П., Преображенская А.В. Особенности строения антарктического ледникового покрова в районе станции Восток по результатам петроструктурных исследований ледяного керна // Проблемы Арктики и Антарктики. 2007. № 2 (76). С. 68–77.

Сербин Д.В., Дмитриев А.Н. Экспериментальные исследования теплового способа бурения плавлением скважины в ледовом массиве с одновременным контролируемым расширением ее диаметра // Записки Горного института. 2022. Т. 257. С. 833–842. https://doi.org/10.31897/PMI.2022.82

Верес А.Н., Екайкин А.А., Липенков В.Я., Туркеев А.В., Ходжер Т.В. Первые данные о климатической изменчивости в районе ст. Восток (Центральная Антарктида) за последние 2000 лет по результатам изучения снежно-фирнового керна // Проблемы Арктики и Антарктики. 2020. 66 (4). С. 482–500. https://doi.org/10.30758/0555-2648-2020-66-4-482-500

Blott S.J., Pye K. Particle shape: a review and new methods of characterization and classification // Sedimentology. 2007. 55 (1). P. 31–63. https://doi.org/10.1111/j.1365-3091.2007.00892.x

Clarke G.K.C. A short history of scientific investigations on glaciers // Journ. of Glaciology. 1987. № 33 (S1). P. 4–24. https://doi.org/10.3189/S0022143000215785

Dengaev A.V. Mechanical Impurities Carry-Over from Horizontal Heavy Oil Production Well // Processes. 2023. № 11. P. 2932. https://doi.org/11.2932.10.3390/pr11102932

Ekaykin A.A., *Lipenkov V.Ya.*, *Tebenkova N.* Fifty years of instrumental surface mass balance observations at Vostok Station, Central Antarctica // Journ. of Glaciology. 2023. P. 1–13. https://doi.org/10.1017/jog.2023.53

Gibson C. RAM-2 Drill system development: an upgrade of the Rapid Air Movement Drill // Annals of Glaciology. 2020. V. 62 (84). P. 1–10. https://doi.org/10.1017/aog.2020.72

Goodge J.W., Severinghaus J.P., Johnson J., Tosi D., Bay R. Deep ice drilling, bedrock coring and dust logging with the Rapid Access Ice Drill (RAID) at Minna Bluff, Antarctica // Annals of Glaciology. 2021. V. 62. P. 1–16. https://doi.org/10.1017/aog.2021.13

Hu Zh., Talalay P.G., Zheng Zh., Cao P., Shi G., Li Y., Fan X., Ma H. Air reverse circulation at the hole bottom in ice-core drilling // Journ. of Glaciology. 2019. V. 65. P. 149–156. https://doi.org/10.1017/jog.2018.95

Hong J., Fan X., Liu Y., Liu G., Liu B., Talalay P. Size distribution and shape characteristics of ice cuttings produced by an electromechanical auger drill // Cold Regions Science and Technology. 2015. V. 119. P. 204–210. https://doi.org/10.1016/j.coldregions.2015.08.012

Hong J., Talalay P., Sysoev M., Fan X. DEM modeling of ice cuttings transportation by electromechanical auger core drills // Annals of Glaciology. 2014. V. 55 (68). P. 65–71. https://doi.org/10.3189/2014AoG68A002

Hou Zh., Liu Y., Meng Q., Xu H., Liang N., Yang G. Investigation of the dynamic ascent characteristics of ice core during polar core drilling // Cold Regions Science and Technology. 2024. 222. 104184. https://doi.org/10.1016/j.coldregions.2024.104184

International Organization for Standardization. ISO 13322–1:2014 Particle size analysis – Image analysis methods – Part 1: Static image analysis methods, 2nd ed. Geneva: International Organization for Standardization, 2014.

International Organization for Standardization. ISO 9276–1:1998 Representation of results of particle size analysis – Part 1: Graphical representation, 2nd ed. Geneva: International Organization for Standardization, 1998.

Kern J., Montagna G., Borges M. Techniques for determining size and shape of drill cuttings // Brazilian Journal of Petroleum and Gas. 2022. V. 16 (2). P. 6577. https://doi.org/10.5419/bjpg2022-0006

Kyzym I., Reyes R., Rana P., Molgaard J., Butt S. Cuttings Analysis for Rotary Drilling Penetration Mechanisms and Performance Evaluation // Conference: ARMA 2015. 49th US Rock Mechanics. 2015.

Litvinenko V.S. Foreword: Sixty-year Russian history of Antarctic sub-glacial lake exploration and Arctic natural resource development // Geochemistry. 2020. 80 (3). https://doi.org/10.1016/j.chemer.2020.125652

Litvinenko V.S., Leitchenkov G.L., Vasiliev N.I. Anticipated sub-bottom geology of Lake Vostok and technological approaches considered for sampling // Geochemistry. 2020. 80. https://doi.org/10.1016/j.chemer.2019.125556

Merkus H.G. Particle Size Measurements Fundamentals, Practice, Quality. Springer, 2009.

Mikhalenko V., Kutuzov S., Toropov P., Legrand M., Sokratov S., Chernyakov G., Lavrentiev I., Preunkert S., Kozachek A., Vorobiev M., Khairedinova A., Lipenkov V. Accumulation rates over the past 260 years archived in Elbrus ice core, Caucasus // Climate of the Past. 2024. V. 20. P. 237–255. https://doi.org/10.5194/cp-20-237-2024

Ren Z., Gao H., Luo W., Elser J. Bacterial communities in surface and basal ice of a glacier terminus in the headwaters of Yangtze River on the Qinghai–Tibet Plateau // Environmental Microbiome. 2022. № 17 (12). P. 1–14. https://doi.org/10.1186/s40793-022-00408-2

Rodriguez J., Edeskär T., Knutsson S. Particle shape quantities and measurement techniques: a review // The electronic journal of geotechnical engineering. 2013. 18. P. 169–198.

Talalay P.G. Removal of cuttings in deep ice electromechanical drills // Cold Regions Science and Technology. 2006. 44 (2). P. 87–98. https://doi.org/10.1016/j.coldregions.2004.08.005

Talalay P.G. Mechanical Ice Drilling Technology. Singapore: Springer, 2016.

Veres A.N., Ekaykin A.A., Golobokova L.P., Khodzher T.V., Khuriganowa O.I., Turkeev A.V. A record of volcanic eruptions over the past 2,200 years from Vostok firn cores, central East Antarctica // Front. Earth Science. 2023. № 11. P. 1075739. https://doi.org/10.3389/feart.2023.1075739

Zhang Z., Lan X., Wen G., Qingming L., Yang X. An Experimental Study on the Particle Size and Shape Distribution of Coal Drill Cuttings by Dynamic Image Analysis // Geofluids. 2021. P. 1–11. https://doi.org/10.1155/2021/5588248